Proceedings of the ASME 2025 20th International Manufacturing Science and Engineering Conference MSEC2025
June 23-27, 2025, Greenville, South Carolina

MSEC2025-155691

ADDITIVE MANUFACTURING WITH CONTINUOUS FIBER: A COMPARISON BETWEEN PREPREG AND IN-SITU IMPREGNATED FIBER ON PRINTING ACCURACY, BONDING, AND MECHANICAL PERFORMANCE

Ziyi Xu[1], Shuaiyin He[1], Koukou Luo[1], Siqi Chen[1], Molong Duan[1,2,*]

[1]Hong Kong University of Science and Technology, Hong Kong SAR, China
[2]HKUST Shenzhen-Hong Kong Collaborative Innovation Research Institute, Futian, Shenzhen, China

ABSTRACT

Continuous fiber-reinforced composites are widely used in aerospace, sports, and energy industries due to their lightweight, high stiffness, and strength. Traditional manufacturing methods for these composites are costly and result in uniform fiber directions. Additive manufacturing, particularly material extrusion, offers a cost-effective alternative for complex shapes, allowing greater freedom in fiber distribution and orientation, thus exploiting fiber anisotropy. Most commercial printers use prepreg fiber for its superior bonding with the matrix and low void content. However, its production involves matrix impregnation, increasing bending stiffness and stress during printing. Conversely, dry fiber and in-situ impregnation systems are favored in research for their ease of construction and fiber deformability. Dry fiber undergoes short-term impregnation in the printer nozzle, reducing stress but compromising bonding quality. Despite their respective advantages, a comprehensive comparison of printed fiber configurations, path accuracy, layer bonding, and mechanical properties for these fibers is lacking. This paper addresses this gap by constructing an in-situ impregnation printer for dry fiber and using the Anisoprint Composer A4 for prepreg fiber, ensuring identical material properties and printing parameters. The study evaluates printing quality through a rich curvature path with varying radii, assessing accuracy via Hausdorff distance and examining layer bonding and fiber configuration using SEM. Mechanical performance is tested with tensile and three-point bending tests on specimens with uni-directional fiber distributions. The tensile test assesses stiffness and strength, while the bending test evaluates inter-layer bonding. The comparative analysis reveals detailed insights into the printing quality and mechanical performance of both fiber types. The key finding is that dry fibers with in-situ impregnation excel at maintaining ideal printing shapes, although their impregnation with the matrix can be poor and introduces defects that reduce product performance. This trade-off provides valuable guidance for fiber and printing system selection in research and industry.

Keywords: additive manufacturing, continuous carbon fiber, printing quality

1. INTRODUCTION

Continuous fiber-reinforced composites are widely adopted in sports, automotive, aerospace, and energy applications due to their lightweight, high stiffness, and strength [1]. Standard fiber-reinforced composites, such as laminate sheets and tubes, benefit from efficient and cost-effective mass production through conventional methods like pultrusion, filament winding, and co-weaving [2]. However, for geometrically complex parts, these traditional methods (e.g., manual layup, resin transfer molding, spray deposition, and vacuum bagging) require expensive molds and result in uniform fiber directions [3]. These limitations are unsuitable for customized production and do not fully exploit the fibers' anisotropic properties. Manipulating local fiber distribution and orientation is increasingly popular for tailoring the mechanical properties of manufactured parts regionally and directionally [4]. These manipulations optimize parts with complex requirements, such as enhanced stiffness/strength [5], reduced fiber usage [6], and tailored frequency response [7]. Material extrusion (MEX) with continuous fiber is a novel manufacturing method that allows for greater deformation of fibers, achieving higher path degrees of freedom [8–11]. Compared to MEX with short fiber [12,13], MEX with continuous fiber significantly enhances the mechanical

* Corresponding author: duan@ust.hk

properties of composites due to the continuity and controllable fiber directions [14–17].

Despite its potential, MEX with continuous fiber is still developing in terms of printing quality, attracting significant research attention. Unlike MEX with polymers, where the material is extruded as a liquid, continuous fiber is solid, and its printing quality can be affected by fiber type, path shape, and printing parameters. To address this, researchers have examined fiber path defects like undulation, twisting, and peeling, considering printing parameters and path curvature. Yamawaki et al. [18] explored the effects of fiber diameter and layer height on path precision. Sugiyama et al. [19] found that shape precision decreases with larger path curvature and fiber bundles. Matsuzaki et al. [20] studied the effects of printed circle diameter and fiber bundle size on printing quality, developing a model to predict actual printed diameter.

These studies focused on fiber bundle size, layer height, and path curvature, but the fiber layout within the bundle also impacts product quality. Bonding methods between fiber and matrix, including pre-impregnation and in-situ impregnation [21], influence fiber layout. Prepreg fiber is commonly used in commercial printers like Anisoprint and Markforge. It is typically impregnated with a thermoset resin, offering a higher fiber volume ratio and better matrix bonding. This resin fixes the fiber layout before extrusion, increasing bending stiffness and limiting deformability, potentially causing twisting and undulation during printing. In contrast, in-situ impregnation simultaneously achieves impregnation and extrusion using dry fiber [22]. The fiber layout is fixed at the nozzle, and lower bending stiffness may enhance deformability for complex paths. Several MEX methods based on in-situ impregnation have been proposed. Matsuzaki et al. [23] developed a printer that pre-heats dry fiber before nozzle feeding. Tian et al. [22] optimized printing parameters to improve quality and mechanical properties. Li et al. [24] used a sizing agent to strengthen the material interface, assuming in-situ impregnation's fiber volume ratio. Yan et al. [25] investigated the shear behavior of fiber-matrix interfaces using standard shear tests and SEM. However, these researches mainly focus on the dry fiber and printing parameters. A direct comparison between prepreg and dry fibers regarding printing accuracy, bonding, and mechanical performance remains necessary.

This paper systematically compares the printing accuracy, bonding, and mechanical performance of prepreg and dry fibers with in-situ impregnation. A printer with an in-situ impregnation extrusion system is employed for dry fiber, and the Anisoprint Composer A4 is employed for prepreg fiber. Identical material properties and printing parameters are set to avoid irrelevant variables. The comparison encompasses studies of printing quality and mechanical performance. For printing quality, a rich curvature path with varying arc radii assesses path accuracy under different curvatures. Single-layer path contours are analyzed and compared to designed paths using image processing, with errors quantified by the Hausdorff distance. Multi-layer paths are sectioned to examine arc cross-sections via SEM for insights into layer bonding and fiber configuration. In the mechanical performance study, specimens with longitudinal and transverse fiber distributions undergo tensile and three-point bending tests. Tensile tests assess stiffness and strength for specimens with longitudinal fiber distributions. Bending tests evaluate inter-layer bonding for both specimen types. These studies provide a detailed assessment of printing quality and mechanical performance for prepreg and dry fibers with in-situ impregnation, highlighting their advantages. The comparison offers valuable guidance for selecting fibers and designing printing systems in research and industry contexts.

2. MATERIALS AND METHODS

2.1. Material and process parameters for printing

The in-situ impregnation 3D printer is designed for dry fiber, and Composer A4 from Anisoprint Corp. is used for prepreg fiber. To ensure that irrelevant variables do not influence the results, both printers use polylactide (PLA/1.75 mm) from eSun Corp. in China as the matrix material. The T300-1K carbon fiber (1000 fibers per bundle) from TENAX-J Corp. in China is used for both prepreg and dry fibers. The prepreg fiber has a diameter of 0.36 mm. The printing process parameters are standardized across both printers and listed in TABLE 1. These parameters are mainly based on the recommendation for Composer A4 from Anisoprint, which has been proven to achieve good print quality and reduces the effort required to optimize parameters. The extrusion ratio of the dry fibers with in-situ impregnation is determined by the pre-printing experiment for the developed printer. The experiment first establishes an extrusion ratio range to prevent fiber bonding failure at low ratios and nozzle clogging due to matrix accumulation at high ratios. Within this range, the extrusion ratio is further fine-tuned to achieve an impregnated fiber printing path size similar to that of Composer A4. This ensures a matrix coating on the dry fibers similar in width and height to that of prepreg fibers, minimizing potential inter-path and inter-layer void discrepancies arising from differing fiber adhesion properties.

TABLE 1: PARAMETERS OF PRINTERS FOR PREPREG AND DRY FIBER

Nozzle diameter	1 mm
Printing speed	1 mm/s
Nozzle Temperature	210°C
Plate Temperature	40°C
Layer height	0.35 mm
Hatching space	1 mm
Extrusion ratio (prepreg)	0.0266 mm/mm
Extrusion ratio (dry)	0.085 mm/mm

2.2. Printer frame and firmware modification

The in-situ impregnation 3D printer designed for dry fiber printing needs to exhibit stable performance comparable to commercial printers. Therefore, the open-source and widely adopted operating system and printer framework are selected. A Raspberry Pi serves as the host computer, controlling the BTT SKR E3 V3 printer control board via the Klipper Mainsail OS, which supports Marlin firmware. The printer framework is based on the Ender 6 from Creativity Corp., and the motion commands are transferred from the modified operating system (FIGURE 1). The performance parameters of the developed printer are listed in TABLE 2.

FIGURE 1: DATA FLOW MODIFICATION TO AN ENDER 6 COMMERCIAL MEX PRINTER

TABLE 2: THE PARAMETERS OF THE IN-SITU IMPREGNATION 3D PRINTER

Build volume [mm]	250 × 250 × 400
Z-axis resolution [mm]	0.1
XY-axes max speed [mm/s]	80
Heater	24 V 60 W Ceramic
Sensor	104NT-4-R025H42G
Nozzle Temperature [°C]	< 300
Nozzle adapter	M6

2.3. In-situ impregnation printing head design

The in-situ impregnation of dry fibers requires the creation of a melt pool for the matrix material within the printing head, allowing the fibers to be fully saturated during passage. Unlike prepreg fibers having higher bending stiffness, the extrusion of dry fibers is achieved through adhesion to the print bed and the movement of the print head, eliminating the need for a dedicated feeding system. To meet this structural requirement, a printing head with a cavity space and dual inlets is designed. The heating block of the printing head employs an annular ceramic heater CHC-V6 and creates the melt pool of the matrix material in a semi-open cavity. This design reduces the overall heating volume, enhancing heating efficiency and control stability. The open melt pool allows for easier observation and cleaning of the molten matrix material, while also decreasing the probability of damage to the dry fibers during impregnation through the cavity. The feeding inlet for the dry fibers is also modified to direct the fibers closer to the nozzle, thereby reducing additional tension caused by the feeding angle and further protecting the dry fibers. The in-situ impregnation printing head is shown in FIGURE 2(B), and its parameters are listed in TABLE 2.

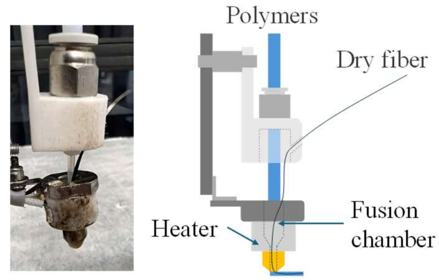

FIGURE 2: SUBSTANCES AND STRUCTURES OF IN-SITU IMPREGNATION PRINTING HEAD

2.4. Printing quality study

Since carbon fibers are solid, they are more susceptible to the influence of the nozzle and the printing path compared to thermoplastic materials during the printing process. The friction between the nozzle and the fibers may affect the quality of matrix bonding on the fibers, particularly in printers utilizing in-situ impregnation, where the matrix on the fiber surface may be scraped off by the nozzle. In this study, segments of straight paths printed with both prepreg and dry fibers with in-situ impregnation will be sectioned and examined using a scanning electron microscope (SEM) to analyze the surface and cross-sectional conditions of the fibers after passing through the nozzle. Arcs in the printing path may cause fiber misalignment or warping, which can be particularly pronounced for prepreg fibers with higher bending stiffness. This study designs a rich curvature printing path (FIGURE 3) incorporating arcs of varying radius and conducts both single-layer and multi-layer printing along this path. The single-layer printing allows for the observation of misalignment in the paths of both prepreg and dry fibers with in-situ impregnation. The printed paths are extracted from images using image processing techniques and compared with the designed path. To calculate the error between the printed path and the designed trajectory, the corresponding circular arcs of the two trajectories are treated as subsets in a metric space. The Hausdorff distance is introduced to evaluate the similarity between these circular arc shapes. Since comparing circular arc trajectories requires a consistent position on the printing path, the Hausdorff distance effectively reflects the topological structure and captures shape features, providing a comprehensive and accurate shape comparison. The Hausdorff distance d_{H} is employed to evaluate the degree of path misalignment and is given by

$$d_{\mathrm{H}}(X,Y) = \max\left\{\sup_{x\in X}\ \inf_{y\in Y}\ d(x,y),\ \sup_{y\in Y}\ \inf_{x\in X}\ d(x,y)\right\}, \quad (1)$$

where X and Y are the contours of printing path and designed path, the points on the contours are x and y, the distance between two points is $d(x,y)$. The multi-layer printed paths will be sectioned to obtain cross-sections at the arcs. These cross-sections will be examined using an SEM to analyze the fiber arrangement, thereby assessing the interlayer bonding quality in multi-layer printing.

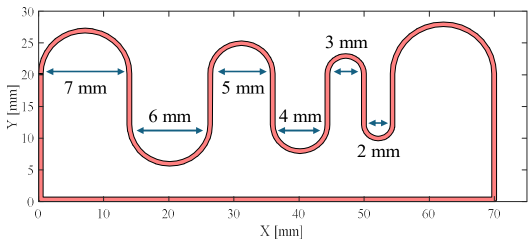

FIGURE 3: DESIGNED RICH CURVATURE PATH

2.5. Mechanical performance study

The mechanical performance of printed products can be affected by defects such as voids or delamination arising from printing quality, making it a crucial metric for comparing the two types of fibers. In this study, rectangular specimens (FIGURE 4) with fibers unidirectionally aligned along their length were printed for tensile and three-point bending tests. The specimen contain 6 layers with 10 fiber bundles per layer. The tensile test evaluates the impact of printing defects on the stiffness and strength of the products, while the three-point bending test compares the interlayer bonding quality of products printed with the two types of fibers. For each test, three specimens are prepared to obtain the average value of the results.

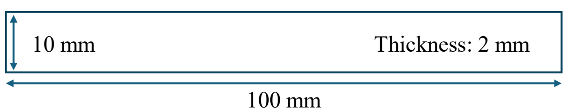

FIGURE 4: RECTANGULAR SPECIMEN

3. RESULTS AND DISCUSSION

3.1. Printing quality study

3.1.1. Printed straight fiber path

The surface and cross-sectional conditions of the fiber paths observed through SEM are illustrated in FIGURE 5. For prepreg fibers, the fiber bundles maintain a circular shape in the cross-section, with tight bonding between fiber and matrix, and the matrix encapsulation on the fiber surface is intact, with no fiber exposure. In contrast, the cross-section of dry fibers with in-situ impregnation is irregular with noticeable voids, and the fiber surfaces are not adequately encapsulated by the matrix. This comparison indicates that the matrix impregnation of dry fibers with in-situ impregnation is suboptimal due to the shorter impregnation time in the print head, leading to higher porosity and poorer interlayer bonding quality in the printed products.

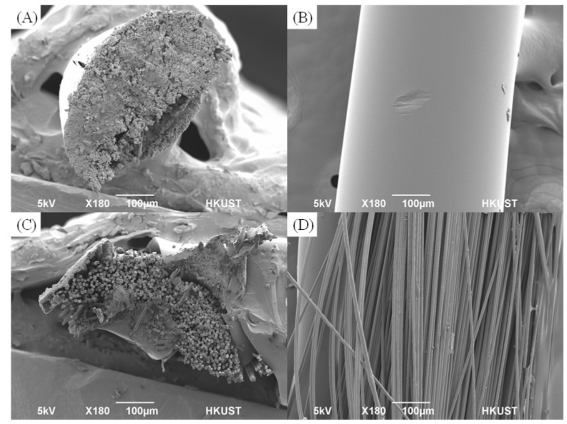

FIGURE 5: THE OBSERVATION OF PREPREG FIBER (A) CROSS-SECTION, (B) SURFACE AND DRY FIBER WITH IN-SITU IMPREGNATION (C) CROSS-SECTION, (D) SURFACE

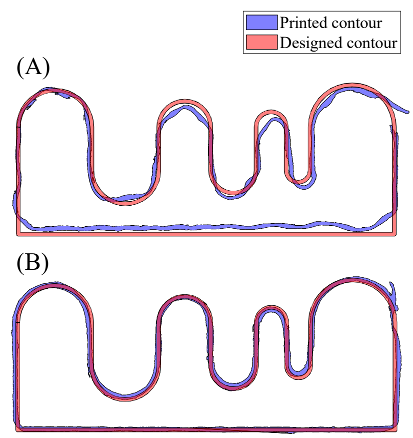

FIGURE 6: THE ALIGNED CONTOURS OF (A) PREPREG FIBER AND (B) DRY FIBER WITH IN-SITU IMPREGNATION

3.1.2. Single layer rich curvature path

The single-layer rich curvature path is photographed using a calibrated camera after printing. The images are converted to grayscale in MATLAB, and the fiber contours are extracted using a contour method. After aligning the extracted contours with the designed path's center, the Hausdorff distance for each arc segment is calculated. The aligned contours are shown in FIGURE 6 and the misalignment results are presented in FIGURE 7. The results indicate that as the arc radius decreases, the fiber misalignment gradually increases. Notably, the misalignment for prepreg fibers is significantly greater than for dry fibers with in-situ impregnation at each arc, and it exhibits fluctuations with changes in arc radius. This may be attributed to the higher bending stiffness of prepreg fibers, which can affect surface smoothness and interlayer fiber bonding during printing. In contrast, the misalignment of dry fibers with in-situ impregnation is smaller and more stable, although there is a noticeable increase at a radius of 7 mm. This may result from insufficient matrix impregnation in the dry fibers, causing displacement during movement along larger arcs.

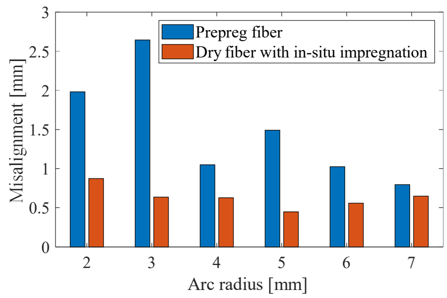

FIGURE 7: THE HAUSDORFF DISTANCE OF THE EXTRACTED CONTOURS TO THE DESIGNED CONTOUR

FIGURE 8: PRINTED MULTI-LAYER PATHS OF (A) PREPREG FIBER AND (B) DRY FIBER WITH IN-SITU IMPREGNATION

3.1.3. Multi-layer rich curvature path

The printing results of the multi-layer rich curvature paths are shown in FIGURE 8. It can be observed that the surface smoothness of the paths printed using prepreg fibers is relatively poor, with noticeable gaps between layers. A waterjet was used to cut arcs for cross-sectional observation. For ease of observation, the section is rotated 90 degrees, from right to left for the printing layer stacking direction. For prepreg fibers (FIGURE 9), misalignment and delamination of fiber bundles were observed across multiple arc sections. The most pronounced effect is at the place (I) from the arc with a radius of 2 mm (FIGURE 9(A)), where can observe three bundles of the prepreg fiber bifurcation. The wall thickness of the 3 mm radius arc (FIGURE 9(B)) is 2.34 mm which is significantly larger than the nozzle diameter. This may be attributed to the smaller curvature causing the prepreg fibers to warp, potentially affecting the strength of the product's curved surface. At the arc with a radius of 4 mm (FIGURE 9(C)), an obvious void is observed at place (II), which may be caused by the misalignment of the fiber bundles. The close view of the fiber bundle (circled by the red dotted line) shows that the prepreg fiber diameter is stable and close to the original diameter for each arc, except for the 2 mm-radius arc. The difference may be caused by the compression of the fiber bundle during printing under small curvature. In the close view of FIGURE 9(B) and (C), debonding between the prepreg fiber and the matrix is observed. This suggests that while the bonding quality within the fiber bundle is good, the surface of the fiber bundle may exhibit poor bonding due to the rapid bonding process during printing. These debondings create voids in the printed part and can lead to fiber bundle pull-out. Consequently, defects are more likely to occur around the fiber bundle rather than inside it. In contrast, the fiber arrangement of dry fibers (FIGURE 10) is more orderly (e.g., the wall thickness of the 3 mm-radius arc is 1.28 mm), which shows the shape of the part is preserved well. However, the cracks on the cross-section are observed at places (III) and (IV) for 2 mm- and 3 mm-radius arcs, which already cause delamination. There is also some interlayer displacement observed at the 4 mm-radius arc (FIGURE 10(C)) due to insufficient matrix impregnation. The voids at places (V), (VI), and (VII) show poor impregnation quality between dry fiber and matrix material. The close view of the fiber bundle shows the irregular shape of fiber, poor impregnation quality can lead to poor load transmitting and fiber pull-out in the bundle, and noticeable voids can lead to the delamination of the part and reduce the strength.

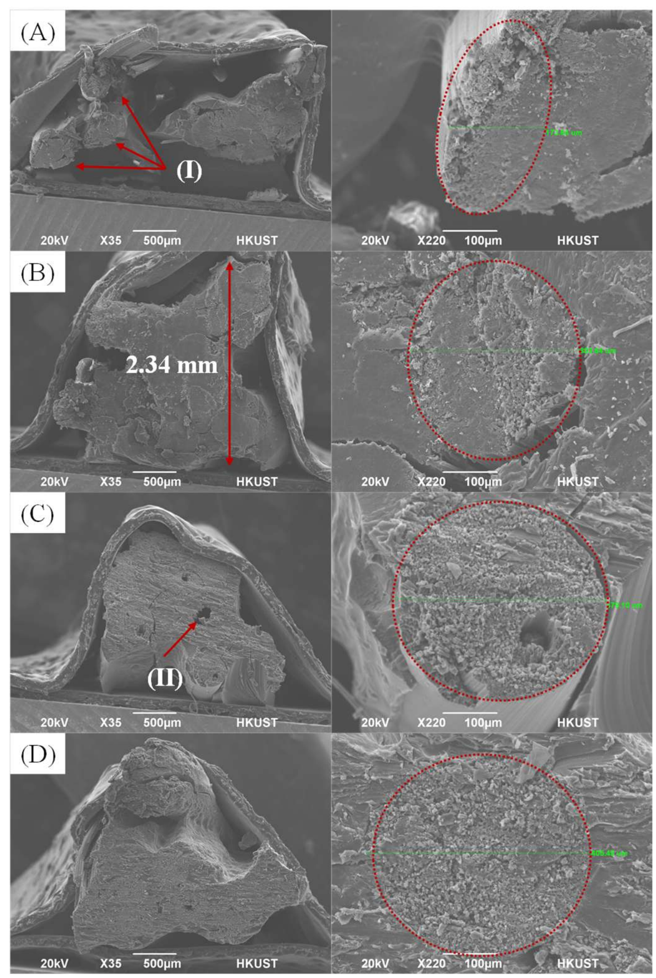

FIGURE 9: PREPREG FIBER ARC CROSS-SECTION AND CLOSE VIEW OF FIBER BUNDLE FOR RADIUS (A) 2 mm, (B) 3 mm, (C) 4 mm, AND (D) 5 mm

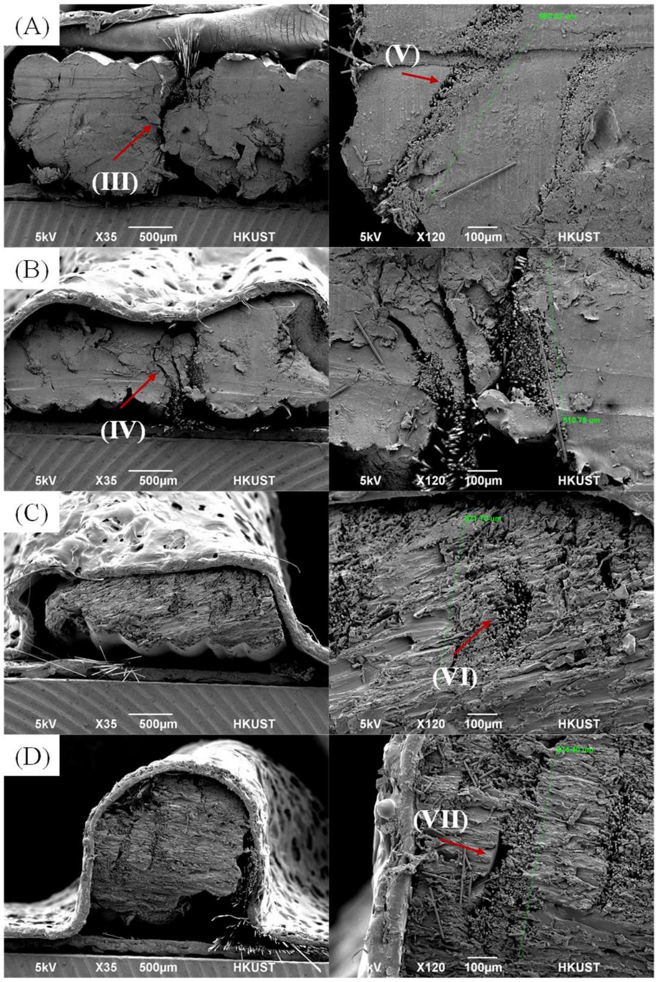

FIGURE 10: DRY FIBER WITH IN-SITU IMPREGNATION ARC CROSS-SECTION AND CLOSE VIEW OF FIBER BUNDLE FOR RADIUS (A) 2 mm, (B) 3 mm, (C) 4 mm, AND (D) 5 mm

3.2. Mechanical performance study

3.2.1. Tensile test

The specimen with uni-directional fiber distribution is printed and shown in FIGURE 11(A) and (B). The tensile test (FIGURE 11(C)) and three-point bending test (FIGURE 11(D)) are performed on the universal testing machine with a testing speed of 1 mm/min. For tensile test, the gauge length is 50 mm. For three-point bending test, the support span is 60 mm. The zoom-in view of the specimens is shown in FIGURE 12, which shows the fiber arrangement in specimens. The load-displacement curve is shown in FIGURE 13 and the calculated stiffness and tensile strength are listed in TABLE 3. Stiffness is the ratio of load to displacement within the linear elastic interval in the experiment result. Strength is the maximum stress calculated by dividing the maximum load by the specimen cross-sectional area. According to the result, the specimens of prepreg fiber and dry fiber with in-situ impregnation have similar stiffness with a 1.93% deviation due to the same type of fiber used for printing. The prepreg fiber specimen achieves 50.4% higher strength compared with that of the dry fiber with in-situ impregnation. The fractures of the specimens (FIGURE 14) show fiber pull-out. The single bundle fracture of prepreg fiber is orderly, because the fiber-matrix bonding quality of prepreg fiber is high, which ensures that the load is transferred to the entire fiber bundle. While in the case of dry fiber with in-situ impregnation, there are scattered fibers of different lengths, which indicates that the matrix does not fully impregnated the interior of the fiber bundle, resulting in uneven load distribution of the fiber bundle. Therefore, the final test strength of dry fiber with in-situ impregnation is lower than that of prepreg fiber. This corresponds to the results of the printing quality study, which shows dry fiber with in-situ impregnation introducing voids poor fiber-matrix bonding to the product. The defects caused by the printing process increase the probability of cracks happening and lead to lower tensile strength.

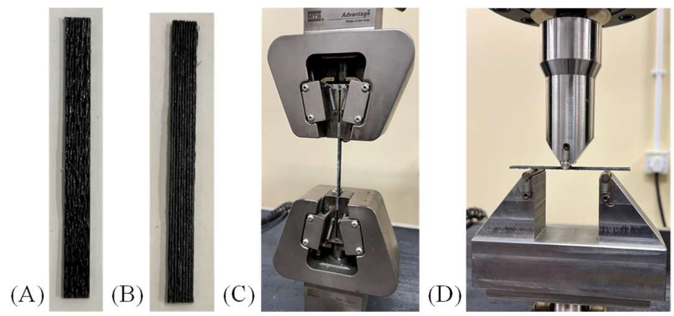

FIGURE 11: PRINTED SPECIMENS OF (A) PREPREG FIBER, (B) DRY FIBER WITH IN-SITU IMPREGNATION, AND SETUP OF (C) TENSILE TEST, (D) THREE-POINT BENDING TEST

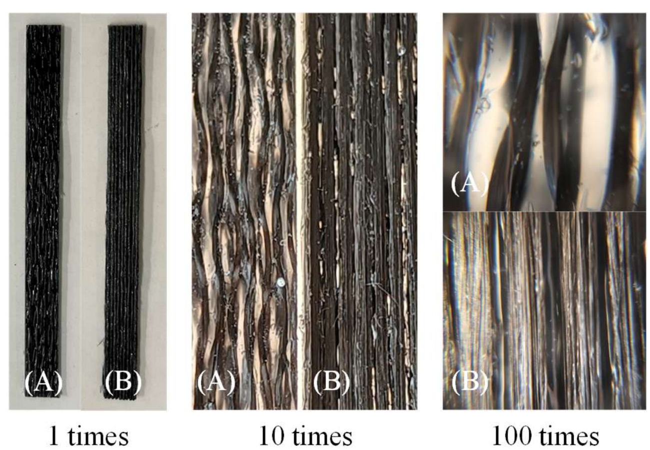

FIGURE 12: ZOOM-IN VIEW OF SPECIMENS OF (A) PREPREG FIBER AND (B) DRY FIBER WITH IN-SITU IMPREGNATION

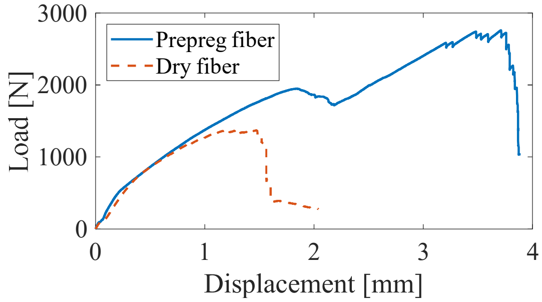

FIGURE 13: LOAD-DISPLACEMENT CURVE OF THE TENSILE TEST

TABLE 3: TENSILE STIFFNESS AND STRENGTH OF TWO KINDS OF FIBERS

	Stiffness [N/mm]	Standard deviation	Strength [N/mm^2]	Standard deviation
Prepreg fiber	1251.767	36.78	137.95	1.57
Dry fiber	1227.573	34.51	68.41	5.38
Deviation	1.93%		50.4%	

FIGURE 14: THE TENSILE FRACTURES OF SPECIMENS OF PREPREG FIBER ON THE LEFT AND DRY FIBER WITH IN-SITU IMPREGNATION ON THE RIGHT

3.2.2. Three-point bending test

The load-displacement curve is shown in FIGURE 15 and the calculated stiffness and tensile strength are listed in TABLE 4. Comparing the bending results, the stiffness and the strength of the specimen of dry fiber with in-situ impregnation are 43.3% and 20% lower than the specimen of prepreg fiber, respectively. Both the fractures of specimens (FIGURE 16) are mainly debonding of fiber and metrix and delamination, but the broken of fiber is observed in the prepreg fiber specimen, which indicates the prepreg fiber carrying more load due to better fiber-matrix bonding compared with the dry fiber with in-situ impregnation. Corresponding to the fiber surface and the multi-layer cross-section observations, the poor impregnation of matrix material, flat fiber bundle shape, and high voids ratio lead to poor bonding quality between layers. The delamination happens during the bending test and leads to the poor mechanical performance of the specimen of dry fiber with in-situ impregnation.

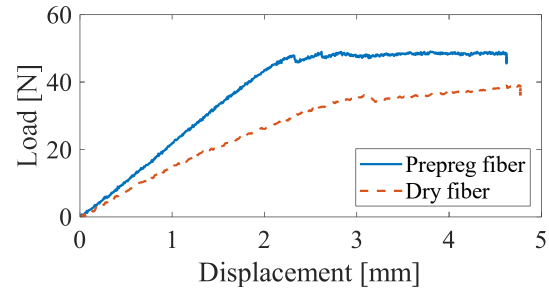

FIGURE 15: LOAD-DISPLACEMENT CURVE OF THE THREE-POINT BENDING TEST

TABLE 4: BENDING STIFFNESS AND STRENGTH OF TWO KINDS OF FIBERS

	Stiffness [N/mm]	Standard deviation	Strength [N/mm^2]	Standard deviation
Prepreg fiber	21.873	1.14	110.48	4.55
Dry fiber	12.412	1.22	88.43	6.79
Deviation	43.3%		20.0%	

FIGURE 16: THE BENDING FRACTURES OF SPECIMENS OF PREPREG FIBER ON THE TOP AND DRY FIBER WITH IN-SITU IMPREGNATION ON THE BOTTOM

4. CONCLUSION

This study compares the printing quality and mechanical performance of prepreg fibers and dry fibers with in-situ impregnation. A printer equipped with an in-situ impregnation printhead was constructed, using identical materials and printing parameters for both fiber types. In the investigation of printing quality, SEM observations of printed straight-line paths were conducted, followed by the printing and analysis of single and multilayer rich curvature paths. The results indicate that prepreg fibers exhibit superior matrix impregnation quality, lower porosity, and better retention of fiber bundle shape compared to dry fibers with in-situ impregnation. However, dry fibers with in-situ impregnation adhere more closely to the ideal path in both single and multilayer curve printing scenarios due to their lower bending stiffness. Corresponding to these studies, tensile tests in the mechanical performance study reveal that while dry fiber with in-situ impregnation specimens exhibit similar tensile stiffness to prepreg specimens, their strength is significantly lower. The results of the three-point bending tests demonstrate that the bending stiffness and strength of dry fiber with in-situ impregnation specimens are inferior to those of prepreg specimens, correlating with the higher porosity and more interlayer cracking observed in the printing quality study. In summary, dry fibers with in-situ impregnation excel at maintaining ideal printing shapes, but their poor impregnation with the matrix leads to numerous defects and reduced product performance. On the other hand, Prepreg fibers exhibit good fiber-matrix bonding, resulting in high stiffness and strength, but their high stiffness necessitates careful path design and printing control to prevent misalignment. For research purposes, dry fibers with in-situ impregnation are easy to integrate into printing systems and offer potential for exploring multi-axis printing paths. In industrial applications, prepreg fibers provide a reliable material for customizing lightweight, high-strength components. Future work could explore the integration of feedback control in the prepreg fiber printing process to adjust real-time printing quality, thereby enhancing adaptability to product shapes while ensuring performance.

ACKNOWLEDGEMENTS

The authors acknowledge support from the Research Grants Council (RGC) of the Government of Hong Kong Special Administrative Region (HKSAR) with the RGC/ECS Project (No. 26215824), HKUST research equipment development fund, HKUST Bridge Gap Fund (BGF), and HKUST Undergraduate Research Opportunities Program (UROP). This work was supported in part by the Project of Hetao Shenzhen-Hong Kong Science and Technology Innovation Cooperation Zone (HZQB-KCZYB 2020083). The help from the funding agency and the other researchers is sincerely appreciated.

REFERENCES

[1] Prashanth, S., Subbaya, K., Nithin, K., and Sachhidananda, S., 2017, "Fiber Reinforced Composites - A Review," J. Mater. Sci. Eng., **06**(03).

[2] Erden, S., and Ho, K., 2017, *Fiber Technology for Fiber-Reinforced Composites*, Elsevier.

[3] Wakeman, M. D., Cain, T. A., Rudd, C. D., Brooks, R., and Long, A. C., 1999, "Compression Moulding of Glass and Polypropylene Composites for Optimised Macro- and Micro-Mechanical Properties II. Glass-Mat-Reinforced Thermoplastics," Compos. Sci. Technol., **59**(5), pp. 709–726.

[4] Blok, L. G., Longana, M. L., Yu, H., and Woods, B. K. S., 2018, "An Investigation into 3D Printing of Fibre Reinforced Thermoplastic Composites," Addit. Manuf., **22**, pp. 176–186.

[5] Hollaway, L. C., 2013, "Advanced Fibre-Reinforced Polymer (FRP) Composite Materials for Sustainable Energy Technologies," *Advanced Fibre-Reinforced Polymer (FRP) Composites for Structural Applications*, Elsevier, pp. 737–779.

[6] He, S., Ma, P.-C., and Duan, M., 2024, "Continuous Fiber Path Optimization in Additive Manufacturing: A Gradient-Based B-Spline Finite Element Approach," Addit. Manuf., **86**, p. 104155.

[7] Tobalina-Baldeon, D., Sanz-Adan, F., Martinez-Calvo, M. A., and Santamaría-Pena, J., 2019, "Dynamic Tensile Stress-Compressive Stress Behavior of Thermoplastic Matrix Composite Materials Reinforced with Continuous Fiber for Automotive Damping and Anti-Vibration Structural Elements," Materials (Basel)., **13**(1), p. 5.

[8] Penumakala, P. K., Santo, J., and Thomas, A., 2020, "A Critical Review on the Fused Deposition Modeling of Thermoplastic Polymer Composites," Compos. Part B Eng., **201**, p. 108336.

[9] Zhuo, P., Li, S., Ashcroft, I. A., and Jones, A. I., 2021, "Material Extrusion Additive Manufacturing of Continuous Fibre Reinforced Polymer Matrix Composites: A Review and Outlook," Compos. Part B Eng., **224**, p. 109143.

[10] Werken, N. Van De, Tekinalp, H., Khanbolouki, P., and Ozcan, S., 2020, "Additively Manufactured Carbon Fiber-Reinforced Composites : State of the Art and Perspective," Addit. Manuf., **31**(November 2019), p. 100962.

[11] Yang, Y., Zhou, Y., and Duan, M., 2024, "Contact-Force-Based Closed-Loop Control of Shell Structure Additive Manufacturing with Continuous-Fiber-Reinforced Polymer Composites," J. Mater. Process. Technol., p. 118501.

[12] Kabir, S. M. F., Mathur, K., and Seyam, A. M., 2020, "A Critical Review on 3D Printed Continuous Fiber-Reinforced Composites : History , Mechanism , Materials and Properties," Compos. Struct., **232**, p. 111476.

[13] Uşun, A., and Gümrük, R., 2021, "The Mechanical Performance of the 3D Printed Composites Produced with Continuous Carbon Fiber Reinforced Filaments Obtained via Melt Impregnation," Addit. Manuf., **46**, p. 102112.

[14] Jiang, D., and Smith, D. E., 2017, "Anisotropic Mechanical Properties of Oriented Carbon Fiber Filled Polymer Composites Produced with Fused Filament Fabrication," Addit. Manuf., **18**, pp. 84–94.

[15] Brenken, B., Barocio, E., Favaloro, A., Kunc, V., and Pipes, R. B., 2018, "Fused Filament Fabrication of Fiber-Reinforced Polymers: A Review," Addit. Manuf., **21**, pp. 1–16.

[16] Heidari-Rarani, M., Rafiee-Afarani, M., and Zahedi, A. M., 2019, "Mechanical Characterization of FDM 3D Printing of Continuous Carbon Fiber Reinforced PLA Composites," Compos. Part B Eng., **175**, p. 107147.

[17] Yuan, S., Li, S., Zhu, J., and Tang, Y., 2021, "Additive Manufacturing of Polymeric Composites from Material Processing to Structural Design," Compos. Part B Eng., **219**, p. 108903.

[18] Yamawaki, M., and Kouno, Y., 2018, "Fabrication and Mechanical Characterization of Continuous Carbon

Fiber-Reinforced Thermoplastic Using a Preform by Three-Dimensional Printing and via Hot-Press Molding," Adv. Compos. Mater., **27**(2), pp. 209–219.
[19] Sugiyama, K., Matsuzaki, R., Ueda, M., Todoroki, A., and Hirano, Y., 2018, "3D Printing of Composite Sandwich Structures Using Continuous Carbon Fiber and Fiber Tension," Compos. Part A Appl. Sci. Manuf., **113**, pp. 114–121.
[20] Matsuzaki, R., Nakamura, T., Sugiyama, K., Ueda, M., Todoroki, A., Hirano, Y., and Yamagata, Y., 2018, "Effects of Set Curvature and Fiber Bundle Size on the Printed Radius of Curvature by a Continuous Carbon Fiber Composite 3D Printer," Addit. Manuf., **24**, pp. 93–102.
[21] Liu, G., Xiong, Y., and Zhou, L., 2021, "Additive Manufacturing of Continuous Fiber Reinforced Polymer Composites: Design Opportunities and Novel Applications," Compos. Commun., **27**.
[22] Tian, X., Liu, T., Yang, C., Wang, Q., and Li, D., 2016, "Interface and Performance of 3D Printed Continuous Carbon Fiber Reinforced PLA Composites," Compos. Part A Appl. Sci. Manuf., **88**, pp. 198–205.
[23] Matsuzaki, R., Ueda, M., Namiki, M., Jeong, T.-K., Asahara, H., Horiguchi, K., Nakamura, T., Todoroki, A., and Hirano, Y., 2016, "Three-Dimensional Printing of Continuous-Fiber Composites by in-Nozzle Impregnation," Sci. Rep., **6**(1), p. 23058.
[24] Li, N., Li, Y., and Liu, S., 2016, "Rapid Prototyping of Continuous Carbon Fiber Reinforced Polylactic Acid Composites by 3D Printing," J. Mater. Process. Technol., **238**, pp. 218–225.
[25] Yan, K., Cao, X., Xie, X., Mei, H., Tang, J., Sun, X., and Ren, F., 2024, "Loading Rate Effect on the Shear Behavior of the Carbon Fiber/Epoxy Interface," Compos. Sci. Technol., **257**, p. 110785.

.